

稀疏孔径一维旋转合成阵列的成像特性

张会燕^{1,2}, 刘明^{1,2*}, 宁布^{1,2,3}, 惠梅^{1,2}, 董立泉^{1,2,3}, 孔令琴^{1,2}, 赵跃进^{1,2}¹北京理工大学光电学院, 北京 100081;²精密光电测试仪器与技术北京市重点实验室, 北京 100081;³北京理工大学长三角研究院(嘉兴), 浙江 嘉兴 314019

摘要 分析了一维多孔径阵列的成像特性,选取子孔径间距比为 1:2 的一维非冗余三孔径结构为基阵列,以最大化频域覆盖为设计标准,设计了沿基线方向对基阵列在 360°范围内以不同角度进行多次旋转的新型合成孔径结构,以提高中频调制传递函数(IFMTF)和系统成像质量。当填充因子为 28.51% 时,旋转合成得到的九孔径阵列的 IFMTF 值(0.1223)大于 Golay-9 阵列的 0.0782。仿真和实验结果的定量和定性评价均证明了所提方法的有效性。

关键词 成像系统; 光学稀疏孔径; 一维多孔径阵列; 旋转合成; 中频调制传递函数; 频域覆盖

中图分类号 O436.1

文献标志码 A

DOI: 10.3788/AOS231668

1 引言

光学稀疏孔径(OSA)成像系统是由多个离散的圆形子孔径经过阵列排布形成的,并以其小的尺寸、低的成本和小的质量来达到等效于大孔径系统的分辨率^[1-2]。但 OSA 系统的光瞳结构具有稀疏性和离散性,系统的调制传递函数(MTF)在中频段会减小甚至降为零,这会导致图像中的部分信息丢失,从而使得采集的图像模糊且对比度低^[3-5]。为了提升中频 MTF 和改善成像质量^[6-7],孔径结构优化设计方法被提出。

在孔径结构优化设计过程中,与单孔径系统相比,稀疏孔径阵列的成像性能强烈依赖于许多结构参数,包括子孔径的数量、相对位置和直径等^[8]。Golay- N (N 为孔径数)孔径结构是设计者通过探究系统的光瞳自相关与光学传递函数之间的关系来寻找具有非冗余和紧凑的二维阵列^[9]。基于 Golay 结构能均匀覆盖频域范围的特性,利用 Fitch 等^[10]提出的分形方法,以 Golay-3 为分形结构单元,钱霖等^[11]设计了由 9 个子镜组成的复合三子镜结构;郝未倩等^[12]按自相似方式扩展设计了多层分形稀疏孔径阵列结构($N=3, 9, 18$);与复合环形结构^[13]相比,当填充因子相同时,刘肖尧等^[14]提出的辐射状多子镜结构具有更大的实际截止频率和实际等效口径,但这些稀疏孔径阵列的子孔径数量较多,实际装配过程比较复杂。以 Golay-6 阵列为基础,易红伟等^[15]采用蒙特卡罗反演方法得到了能形

成均匀一致的频率响应覆盖平面的等边六边形结构,魏小峰等^[16]提出了实现中低频段频谱能量最大化的中心聚合型六孔径阵列。梁士通等^[17]提出了一种在等效直径和 MTF 的均匀性方面均优于三臂结构的九孔径新型稀疏孔径结构。

随着无需梯度信息的新优化算法的出现,为了寻求最大均匀 U-V 平面覆盖的解,Guyon 等^[18]利用模拟退火算法,找到了包含 4~10 个相同望远镜的旋转阵列的最优布局,还证明了这种旋转优化阵列能够恢复复杂光源的图像并获得更多的光谱信息。基于该研究,模拟退火算法^[19-20]、遗传算法^[21-24]、穷举搜索^[25]、混合算法^[26]、端到端^[27]等方法被陆续提出,并对经典二维阵列的结构参数重新进行优化,使其具有更好的成像性能。但以上的优化方法对初始阵列结构具有依赖性。

本文分析了一维多孔径阵列结构的成像性能,以最大化频域覆盖为设计标准,选择子孔径间距比为 1:2 的一维非冗余三孔径结构作为基元阵列,固定中间子孔径位置不变,在 360°范围内沿基线方向以不同角度进行多次旋转,得到新型旋转合成孔径结构。仿真和实验结果都表明所提出的旋转合成孔径阵列提高了稀疏孔径系统的中频 MTF,改善了成像质量。

2 旋转合成孔径的基本原理

2.1 一维多孔径阵列

图 1 给出了一维多孔径阵列($N=2, 3, 4, 5$)的光

收稿日期: 2023-10-17; 修回日期: 2023-12-05; 录用日期: 2023-12-13; 网络首发日期: 2023-12-23

基金项目: 国家自然科学基金(11774031)、国家重点研发项目(2018YFF0300804)、北京理工大学嘉兴长三角研究院研究生创新研究项目(GIIP2022-007)

通信作者: *bit411liu@bit.edu.cn

瞳结构及其自相关分布,其子孔径直径和像平面边长(以五孔径尺寸为标准)都是相同的尺寸,且这 4 种结构都是以最大填充因子 F_{\max} 进行设计的。为保证在频域范围内的覆盖是连续的,设计标准为最大化从原点到自相关分布第一个零点的位置,光瞳结构体现为相邻两子孔径的间距比 S 。从图 1 中可以看出,随着子孔径数量的增多,光瞳结构自相关分布的范围更广,但是强度在减小, $N=5$ 时出现零值,这就意味着 $N \geq 5$ 时一维阵列本身已无法达到基线方向上的频谱覆盖。如果对双孔径($N=2$)结构沿基线方向旋转一次:当固定一个子孔径并绕其旋转 60° 就得到填充因子最大的

Golay-3 结构;当绕相切点旋转两个子孔径 90° 就得到填充因子最大的正四边形结构。但这两种结构的填充因子过大,在实际应用中的制造成本与单孔径相比优势不大。一维三孔径($N=3$)阵列的填充因子分别为四孔径($N=4$)和五孔径($N=5$)阵列的 2 倍和 4 倍以上,即它们至少需要旋转 2 次和 4 次才能达到相同的通光面积,同时子孔径的数量也会翻倍增加,导致结构复杂,成像效率低。因此,为了使系统的 MTF 在最大截止频率内不会出现零值点,同时能够以较少的旋转次数及较小的填充因子获取更大的频域覆盖,本文选取一维非冗余三孔径($N=3$)结构进行合成孔径设计。

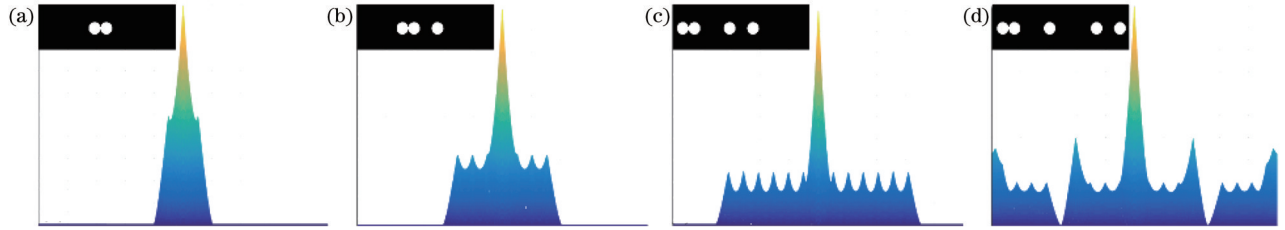


图 1 一维多孔径($N=2, 3, 4, 5$)阵列的光瞳结构及其自相关分布。(a) $N=2, F_{\max}=50\%, S=1$; (b) $N=3, F_{\max}=18.75\%, S=1:2$; (c) $N=4, F_{\max}=8.16\%, S=1:3:2$; (d) $N=5, F_{\max}=4.13\%, S=1:3:4:2$

Fig. 1 One-dimensional multi-aperture ($N=2, 3, 4, 5$) array pupil structures and its autocorrelation distributions. (a) $N=2, F_{\max}=50\%, S=1$; (b) $N=3, F_{\max}=18.75\%, S=1:2$; (c) $N=4, F_{\max}=8.16\%, S=1:3:2$; (d) $N=5, F_{\max}=4.13\%, S=1:3:4:2$

2.2 旋转特性

图 2 给出了在入射光波长为 550 nm 、填充因子为 15.05% 的一维三孔径稀疏阵列的光瞳结构、三维 MTF 和点扩散函数 (PSF) 分布,其中 d 为子孔径直径,三个子孔径的中心位置坐标从左到右依次为

$(-2d/\sqrt{3}, 0), (0, 0), (4d/\sqrt{3}, 0)$, $s_1=2d/\sqrt{3}$ 和 $s_2=2s_1$ 为两个子孔径中心间距, D_{circ} 是最小外接圆直径,即有效直径。从图 2 中可以看出,该结构的 MTF 集中在基线方向,其 PSF 多个旁瓣能量分散了中心能量,因此当该系统进行成像时,会导致严重的图像退化。

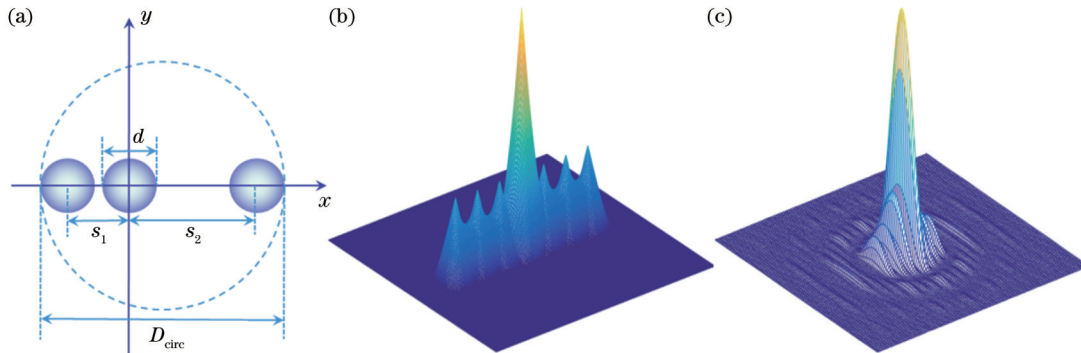


图 2 一维三孔径阵列的光瞳结构、三维 MTF 和 PSF 分布。(a) 光瞳结构; (b) MTF; (c) PSF

Fig. 2 Pupil structure, three-dimensional MTF and PSF distributions of one-dimensional three-aperture array. (a) Pupil structure; (b) MTF; (c) PSF

上述结构的光瞳函数可表示为

$$\begin{aligned}
 P(x, y) &= \text{circ}\left(\frac{\sqrt{x^2 + y^2}}{d/2}\right) \sum_{i=1, j=0}^{i=3, j=k} \delta(x - x_{ij}, y - y_{ij}) = \\
 &\text{circ}\left(\frac{\sqrt{x^2 + y^2}}{d/2}\right) \left[\delta(x - x_{10}, y - y_{10}) + \delta(x - x_{20}, y - y_{20}) + \delta(x - x_{30}, y - y_{30}) \right] = \\
 &\text{circ}\left(\frac{\sqrt{x^2 + y^2}}{d/2}\right) \left[\delta(x, y) + \delta(x + s_1, y) + \delta(x - s_2, y) \right], \quad (1)
 \end{aligned}$$

式中: (x_{ij}, y_{ij}) 为旋转 $j(j=0, \dots, k)$ 次的第 $i(i=1, 2, 3)$ 个子孔径的中心坐标; $\text{circ}(\cdot)$ 为圆域函数; $\delta(x, y)$ 为狄拉克函数。为了方便计算, 中间、左侧和右侧的三个子孔径中心位置坐标分别记为 (x_{10}, y_{10}) 、 (x_{20}, y_{20}) 、 (x_{30}, y_{30}) 。

图 3 给出了旋转角度为 α 、旋转一次的合成孔径的

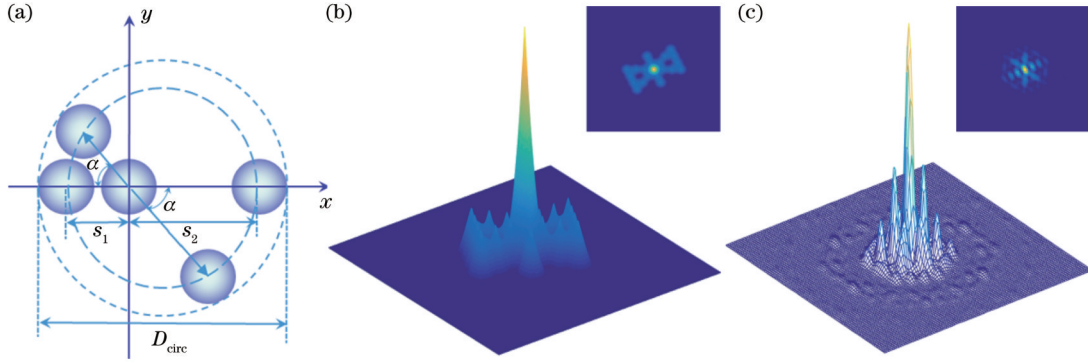


图 3 旋转一次后的光瞳结构, 以及二维和三维的 MTF 和 PSF 分布。(a) 光瞳结构; (b) MTF ($\alpha=2\pi/7$); (c) PSF ($\alpha=2\pi/7$)
Fig. 3 Pupil structure and MTF and PSF distributions in two and three dimensions after one rotation. (a) Pupil structure; (b) MTF ($\alpha=2\pi/7$); (c) PSF ($\alpha=2\pi/7$)

为保证任意两个子孔径之间不会在空间上发生重叠, s_1, s_2 应该满足以下的约束条件:

$$\begin{cases} \left[\delta(x_{ij}, y_{ij}) \Big|_{i=2}^{j=1} \text{circ}(s_1) \right] \cap \left[\delta(x_{ij}, y_{ij}) \Big|_{i=2}^{j=0} \text{circ}(s_1) \right] = 0 \\ \left[\delta(x_{ij}, y_{ij}) \Big|_{i=3}^{j=1} \text{circ}(s_2) \right] \cap \left[\delta(x_{ij}, y_{ij}) \Big|_{i=3}^{j=0} \text{circ}(s_2) \right] = 0 \end{cases} \quad (2)$$

旋转 j 次, 每次的旋转角度 α_j 应满足

$$\begin{cases} \alpha_{\min} = 2\arcsin\left(\frac{r_1}{s_1}\right) \\ k \leq \left\lfloor \frac{2\pi}{\alpha_{\min}} \right\rfloor = 6 \\ \alpha_j = \frac{2\pi}{j+1}, \quad j=0, 1, \dots, 6 \end{cases} \quad (3)$$

因此, 旋转后的子孔径中心位置坐标可表示为

$$\begin{cases} (x_{2j}, y_{2j}) \Big|_{j=0,1,2,3,4,5,6} = (-s_1 \cos \alpha_j, s_1 \sin \alpha_j) \\ (x_{3j}, y_{3j}) \Big|_{j=0,1,2,3,4,5,6} = (s_2 \cos \alpha_j, -s_2 \sin \alpha_j) \end{cases} \quad (4)$$

旋转后得到的新的合成孔径的光瞳函数可表示为

$$\begin{aligned} P_{\text{new}}(x, y) &= \text{circ}\left(\frac{\sqrt{x^2 + y^2}}{d/2}\right) \left[\delta(x, y) + \sum_{j=0}^{j=6} \delta(x - x_{2j}, y - y_{2j}) + \delta(x - x_{3j}, y - y_{3j}) \right] = \\ &= \text{circ}\left(\frac{\sqrt{x^2 + y^2}}{d/2}\right) \left\{ \delta(x, y) + \sum_{j=0}^{j=6} \delta[x - (-s_1 \cos \alpha_j), y - s_1 \sin \alpha_j] + \delta[x - s_2 \cos \alpha_j, y - (-s_2 \sin \alpha_j)] \right\}. \end{aligned} \quad (5)$$

在非相干情况下, PSF 是相干脉冲响应的幅度平方, 用 $P_{\text{SF}}(u, v)$ 表示:

$$\begin{aligned} P_{\text{SF}}(u, v) &= \left| \mathcal{F}\{P_{\text{new}}(x, y)\} \right|^2 = \\ &= \left(\frac{\pi d^2}{4\lambda f} \right)^2 \left[\frac{2J_1(\pi d \sqrt{u^2 + v^2} / \lambda f)}{\pi d \sqrt{u^2 + v^2} / \lambda f} \right]^2 \left| \left\{ 1 + \sum_{j=0}^{j=6} \exp[-i(ux_{2j} - vy_{2j})] + \exp[-i(ux_{3j} - vy_{3j})] \right\} \right|^2, \end{aligned} \quad (6)$$

式中: $\mathcal{F}\{\cdot\}$ 代表傅里叶变换; (u, v) 是像平面坐标; λ 是入射光波长; f 为出瞳面到像面的距离; J_1 是一阶贝塞尔函数。PSF 再经过归一化傅里叶变换得到光学传递函数(OTF):

$$\text{OTF}(f_x, f_y) \equiv \frac{\mathcal{F}\{P_{\text{SF}}(u, v)\}}{\int_{-\infty}^{\infty} \int_{-\infty}^{\infty} P_{\text{SF}}(u, v) dudv}, \quad (7)$$

式中: $f_x = x/\lambda f$ 和 $f_y = y/\lambda f$ 是空间频率。OTF 的模为

MTF_{array} :

$$\text{MTF}_{\text{array}}(f_x, f_y) = \text{MTF}_{\text{sub}}(f_x, f_y) \times \left[\delta(f_x, f_y) + \frac{1}{2j+3} \sum_{j=0}^{j=6} \delta\left(f_x \pm \frac{x_{2j}}{\lambda f}, f_y \pm \frac{y_{2j}}{\lambda f}\right) + \delta\left(f_x \pm \frac{x_{3j}}{\lambda f}, f_y \pm \frac{y_{3j}}{\lambda f}\right) + \delta\left(f_x \pm \frac{x_{3j} - x_{2j}}{\lambda f}, f_y \pm \frac{y_{3j} - y_{2j}}{\lambda f}\right) \right], \quad (8)$$

式中: MTF_{sub}为单个子孔径的 MTF, 可以表示为

$$\text{MTF}_{\text{sub}}(f_x, f_y) = \begin{cases} \frac{2}{\pi} \left[\arccos\left(\frac{\lambda f}{d} \sqrt{f_x^2 + f_y^2}\right) - \frac{\lambda f}{d} \sqrt{f_x^2 + f_y^2} \sqrt{1 - \left(\frac{\lambda f}{d} \sqrt{f_x^2 + f_y^2}\right)^2} \right] & \sqrt{f_x^2 + f_y^2} \leq \frac{d}{\lambda f} \\ 0 & \sqrt{f_x^2 + f_y^2} > \frac{d}{\lambda f} \end{cases}. \quad (9)$$

为了定量评价 IFMTF 的提升效果, 可以用一个单值 $M_{\text{mid-freq}}$ 表示, 定义为 MTF 从单个子孔径截止频率 ρ_d 到实际截止频率 ρ_c 在空间频率上的平均值:

$$M_{\text{mid-freq}} \approx \frac{\int_0^{2\pi} \int_{\rho_d}^{\rho_c} \text{MTF}(\rho, \theta) \rho d\rho d\theta}{\int_0^{2\pi} \int_{\rho_d}^{\rho_c} \rho d\rho d\theta} = \frac{\int_0^{2\pi} \int_{\rho_d}^{\rho_c} \text{MTF}(\rho, \theta) \rho d\rho d\theta}{\pi(\rho_c^2 - \rho_d^2)}. \quad (10)$$

3 旋转合成孔径结构

3.1 单次旋转合成

通过式(3)计算可得, 最先相切的两个子孔径之间的角度最小为 $\alpha_{\min} = 51.336^\circ$, 因此单次旋转的最小角度为 $2\pi/7 (51.429^\circ)$ 。图 4 展示了以 $2\pi/7, \pi/3, 2\pi/5,$

$\pi/2$ 和 $2\pi/3$ 旋转一次后的光瞳结构、MTF 及 PSF 分布。随着单次旋转角度的增大, MTF 和 PSF 的能量主要集中在中心区域, MTF 旁瓣的能量在沿着光瞳结构的两个方向上是连续的, 在其他方向上逐渐呈现出点状的离散分布, 覆盖的频域范围变得更广, PSF 则呈现出较为离散的点状分布。

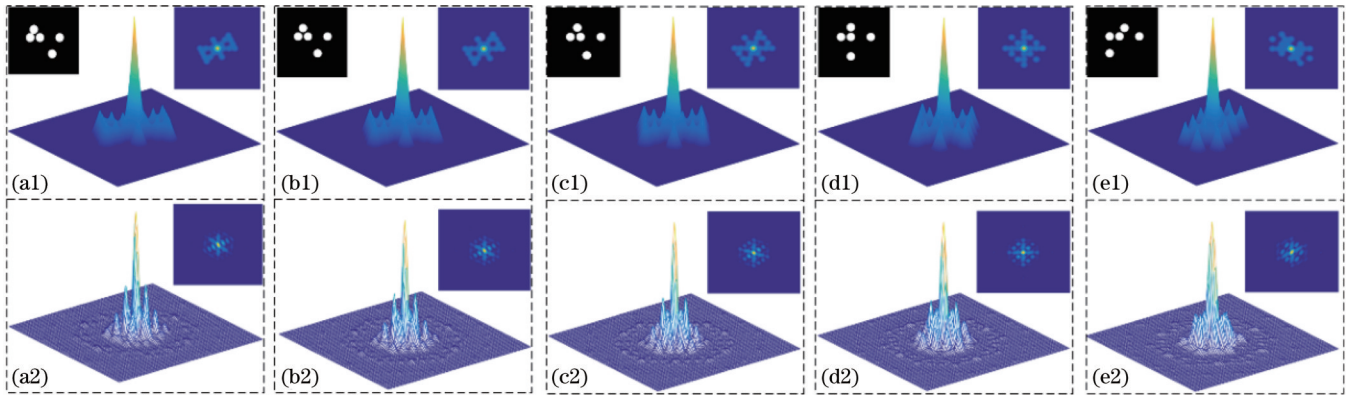


图 4 单次旋转不同角度的光瞳结构、MTF 频谱及 PSF 分布。(a1)(a2) $2\pi/7$; (b1)(b2) $\pi/3$; (c1)(c2) $2\pi/5$; (d1)(d2) $\pi/2$; (e1)(e2) $2\pi/3$

Fig. 4 Pupil structures, MTF spectra, and PSF distributions at different angles of single rotation. (a1)(a2) $2\pi/7$; (b1)(b2) $\pi/3$; (c1)(c2) $2\pi/5$; (d1)(d2) $\pi/2$; (e1)(e2) $2\pi/3$

一次旋转得到的孔径结构不能覆盖整个频域范围, 因此需要进行多次旋转, 在一周内旋转合成新型孔径结构, 旋转的最高次数为 6 次。图 5 给出了旋转一次和多次的子孔径总数及相应的填充因子变化。图 5 (a) 表明: 旋转多次时, 随着单次旋转角度的增大, 子孔径总数和旋转次数变少。从图 5 (b) 可以看出, 旋转一次得到的五孔径阵列的填充因子大于旋转两次得到的七孔径阵列的填充因子, 随着子孔径数目的减小, 旋转多次得到的阵列的填充因子减小。

3.2 多次旋转合成

为了增大旋转合成孔径在整个频域内的覆盖范围, 在 360° 范围内, 分别以每 $2\pi/7$ 旋转 6 次, 每 $\pi/3$ 旋转 5 次, 每 $2\pi/5$ 旋转 4 次, 每 $\pi/2$ 旋转 3 次, 每 $2\pi/3$ 旋转 2 次, 将得到的旋转合成阵列分别记为 OR6、OR5、OR4、OR3、OR2。图 6 展示了 5 种旋转合成阵列和 Golay-9 阵列的光瞳结构, 以及二维和三维的 MTF、PSF 分布。随着旋转次数的减少, 旋转合成孔径的 MTF 频域覆盖范围变小, 并且呈现出了离散化的分

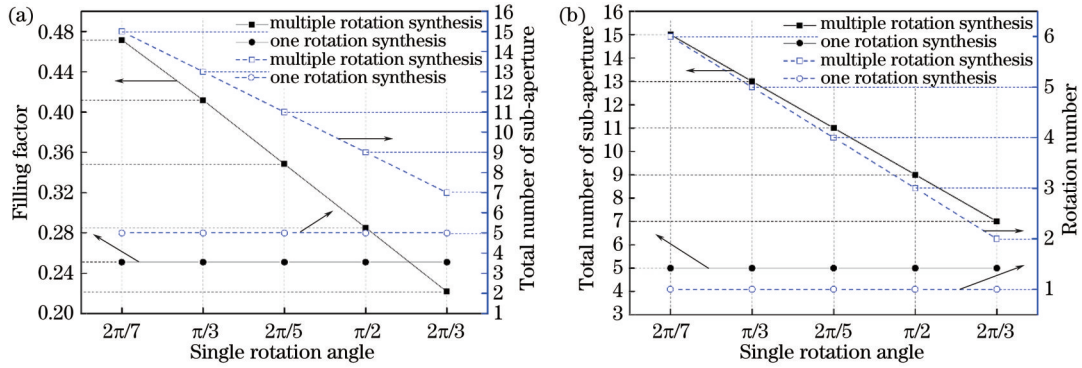


图 5 不同旋转角度下的旋转次数、子孔径总数及填充因子变化。(a)子孔径总数和旋转次数随旋转角度的变化;(b)填充因子和子孔径总数随旋转角度的变化

Fig. 5 Changes of rotation times, total number of sub-apertures, and filling factor under different rotation angles. (a) Total number of sub-apertures and number of rotations varying with rotation angle; (b) filling factor and total number of sub-apertures varying with rotation angle

布,其 PSF 能量主要集中在中心区域,但旁瓣能量逐渐增大。图 6(a3)、(a4)中 OR6 阵列的 PSF 能量几乎全部集中在中心,接近于单孔径的 PSF 分布。图 6(b3)、(b4)和图 6(c3)、(c4)的 OR5 和 OR4 阵列的 PSF 旁瓣都向中心聚拢。但图 6(d3)、(d4)和图 6(e3)、(e4)的

OR3 和 OR2 阵列的 PSF 能量分布更加离散化,旁瓣的能量不断增强,这就导致了成像的模糊。在等效口径相同的情况下,图 6(f1)、(f2)中 Golay-9 阵列的 MTF 分布比较均匀,但其 MTF 的分布在中高频段强度较小,图 6(f3)、(f4)的 PSF 呈现出离散的圆斑分布。

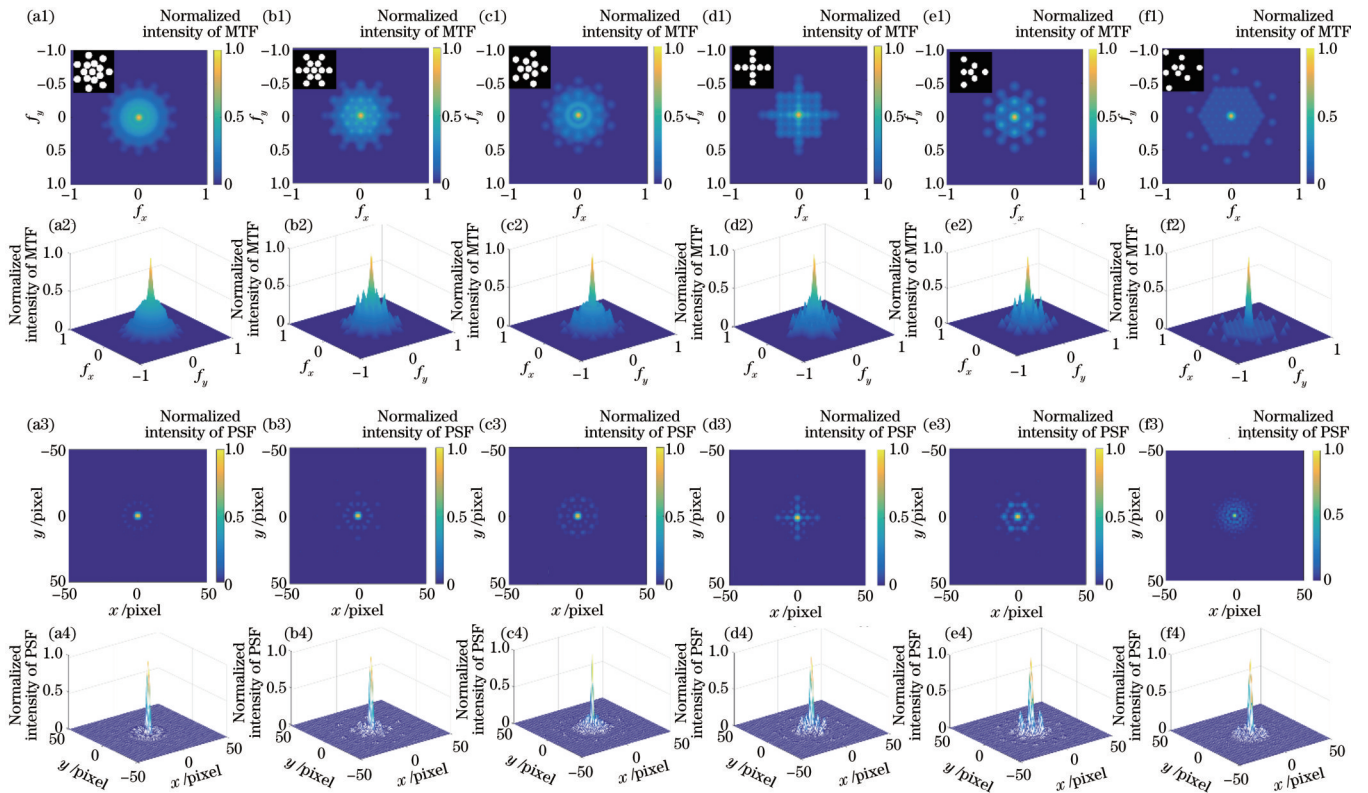


图 6 旋转合成孔径和 Golay-9 阵列的光瞳结构及相应的二维和三维 MTF、PSF 分布。(a1)~(a4)OR6 阵列;(b1)~(b4)OR5 阵列;(c1)~(c4)OR4 阵列;(d1)~(d4)OR3 阵列;(e1)~(e4)OR2 阵列;(f1)~(f4)Golay-9 阵列

Fig. 6 Pupil structures and corresponding two-dimensional and three-dimensional MTF and PSF distributions of rotating synthetic aperture and Golay-9 array. (a1)-(a4) OR6 array; (b1)-(b4) OR5 array; (c1)-(c4) OR4 array; (d1)-(d4) OR3 array; (e1)-(e4) OR2 array; (f1)-(f4) Golay-9 array

图 7 展示了这 5 种旋转合成阵列、单孔径及 Golay-9 阵列的一维 MTF 分布。在 f_x 方向,OR5 和 OR3 阵列

在频率为 0.4~1.0 范围内的 MTF 接近于单孔径的 MTF,且在整体空间频率范围内高于 Golay-9 阵列的

MTF, OR6、OR4 和 OR2 阵列在频率为 0.18~0.6 范围内的 MTF 高于 Golay-9 的 MTF,但在频率 0.8 左右就降低为 0,呈现了截止状态。在 f_y 方向,OR2 阵列的 MTF 波动范围较大,在频率为 0.5 左右就出现了零

值,其他 4 种旋转合成阵列的 MTF 整体上分布均匀,有相似的趋势,且在频率为 0.2~0.6 的范围内均大于 Golay-9 阵列的 MTF,其中 OR3 阵列在 0.15~1.0 频率范围内的 MTF 大于 Golay-9 阵列的 MTF。

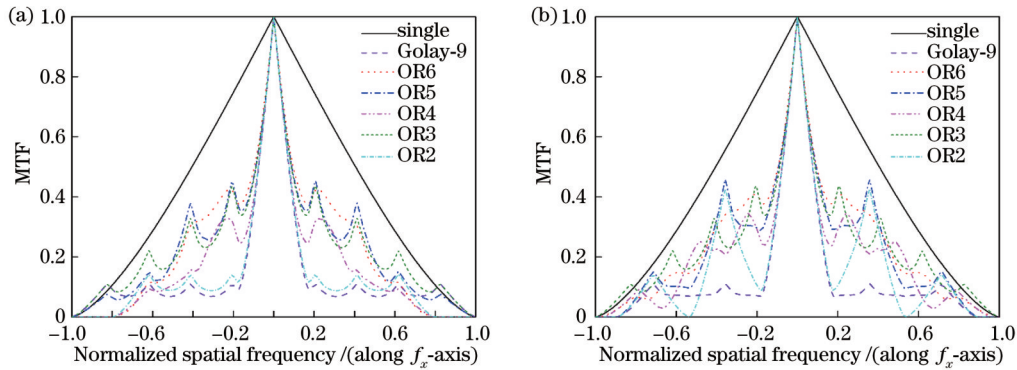


图 7 旋转合成阵列、单孔径和 Golay-9 的一维 MTF 分布。(a)沿 f_x 方向的 MTF;(b)沿 f_y 方向的 MTF

Fig. 7 One-dimensional MTF distributions of rotating synthetic aperture, single aperture, and Golay-9 array. (a) MTF along f_x axis; (b) MTF along f_y axis

图 8 给出了 USAF1951 分辨率板经过 Golay-9、OR4 和 OR3 稀疏孔径成像系统的仿真图像。图 8(a) 为作为参考标准的原始图像。可以观察到,图 8(c)、(d) 的图像比图 8(b) 清晰。数值上,OR4 阵列的峰值信噪比 (PSNR) 为 24.80 dB,高于 Golay-9 阵列的

22.89 dB,其结构相似度 (SSIM) 为 0.7187,也大于 Golay-9 阵列的 0.6149。同样地,OR3 阵列的 PSNR 和 SSIM 也高于 Golay-9 阵列。结果表明,旋转合成孔径阵列能有效提高图像质量。

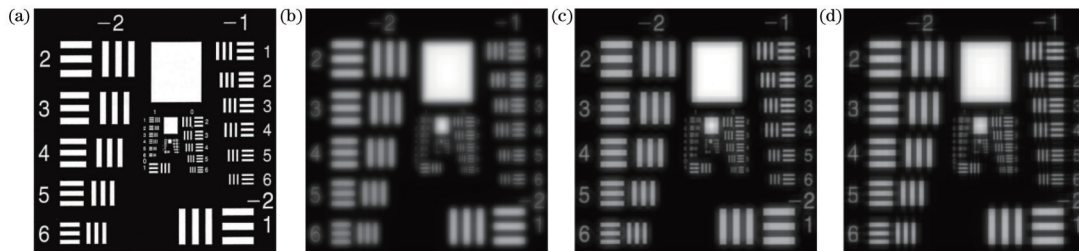


图 8 Golay-9、OR4 和 OR3 阵列的仿真图像。(a)原图;(b) Golay-9 阵列的仿真图像;(c)OR4 阵列的仿真图像;(d)OR3 阵列的仿真图像

Fig. 8 Simulation images of Golay-9, OR4, and OR3 arrays. (a) Original image; (b) simulation image of Golay-9 array; (c) simulation image of OR4 array; (d) simulation image of OR3 array

表 1 列出了单孔径、Golay-9 和旋转合成孔径的成像特性评价指标。旋转合成孔径的 $M_{\text{mid-freq}}$ 、PSNR 和 SSIM 随着填充因子的减小而减小,其中 OR6 阵列的子孔径数量最多,填充因子达到了 47.15%,除了实际截止频率 (0.7901) 低于 OR5 阵列的 0.889,其 $M_{\text{mid-freq}}$ 、PSNR 和 SSIM 都是高于其他旋转合成阵列的,其 $M_{\text{mid-freq}}$ 的 0.136 也最接近等效单孔径的 0.2128,但其子孔径数量较多,且中间圆周上的 7 个孔径几乎相切,实际安装配准过程难度较大。OR5 阵列结构也面临相似的问题,同时 OR5 阵列还是冗余的,两两子孔径之间覆盖的频域范围会发生重叠,不能充分利用稀疏孔径阵列排布的优势。其余的三种旋转合成阵列中,OR4 阵列的 4 种像质评价标准高于其他两个阵列结构,其成像性能接近于 OR5,但其填充因子、子孔径数

目和旋转次数都比 OR5 阵列小,而且 SSIM 是高于 OR5 阵列的。与 Golay-9 阵列相比,当子孔径数量与 Golay-9 阵列相同或更少时,旋转合成孔径可以获得更大的填充因子,除了实际截止频率低于 Golay-9 阵列的 0.8951,其他三种评价指标均高于 Golay-9 阵列的。

4 实验验证

图 9 展示了光学原理图和实验装置图。LED 光源 (550 nm) 照射 USAF1951 分辨率板 (United States MIL-STD-150A),为了与望远系统的成像模型一致,将目标置于平行光管前,以模拟物体在无限远处的成像。在双胶合透镜 (GCL-0106,口径 50.8 mm,焦距 400 mm) 前面放置一个稀疏孔径掩模板,用于调整不

表 1 单孔径、Golay-9 和旋转合成孔径阵列结构的成像特性评价指标

Table 1 Evaluation indexes of imaging characteristics of single aperture, Golay-9, and rotating synthetic aperture array structures

Array	Number of sub-apertures	Filling factor / %	Practical cutoff frequency ρ_c	$M_{\text{mid-freq}}$	PSNR / dB	SSIM
Single	1	100.00	1.0000	0.2128	31.18	0.9563
Golay-9	9	14.00	0.8951	0.0782	22.89	0.6149
OR6	15	47.15	0.7901	0.1360	25.58	0.7577
OR5	13	41.18	0.8889	0.1250	24.91	0.7140
OR4	11	34.84	0.7912	0.1245	24.80	0.7187
OR3	9	28.51	0.6528	0.1223	24.47	0.6910
OR2	7	22.17	0.5309	0.0937	23.22	0.6282

同的阵列结构形式,包括 Golay-9($d=2.4\text{ mm}$, $D_{\text{circ}}=20\text{ mm}$)、OR3($d=3\text{ mm}$, $D_{\text{circ}}=20\text{ mm}$)和 OR4($d=3\text{ mm}$, $D_{\text{circ}}=20\text{ mm}$)阵列结构。光线经过掩模板后被

双胶合透镜会聚到 CMOS 探测器 (BFS-U3-200S6M-C, 5477×3648 阵列, $2.4\text{ }\mu\text{m}$ 像素间距),最终通过计算机进行保存和处理。

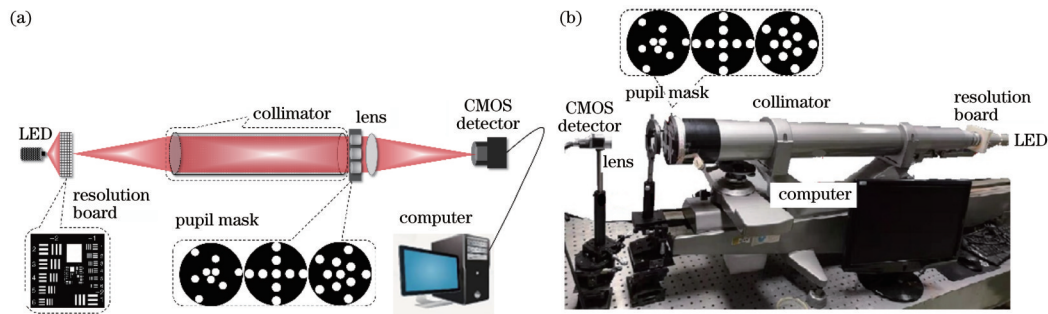


图 9 光路图和实验装置图。(a)光路图;(b)实验装置图

Fig. 9 Optical path diagram and experimental device diagram. (a) Optical path diagram; (b) experimental device diagram

实验对比了 Golay-9、OR3 和 OR4 阵列的成像效果,如图 10 所示。从图 10(a)~(c)可以看出这三种阵

列结构的图像在视觉上的清晰度和对比度从高到低依次为 OR4、OR3、Golay-9。为了获得更准确的对比变

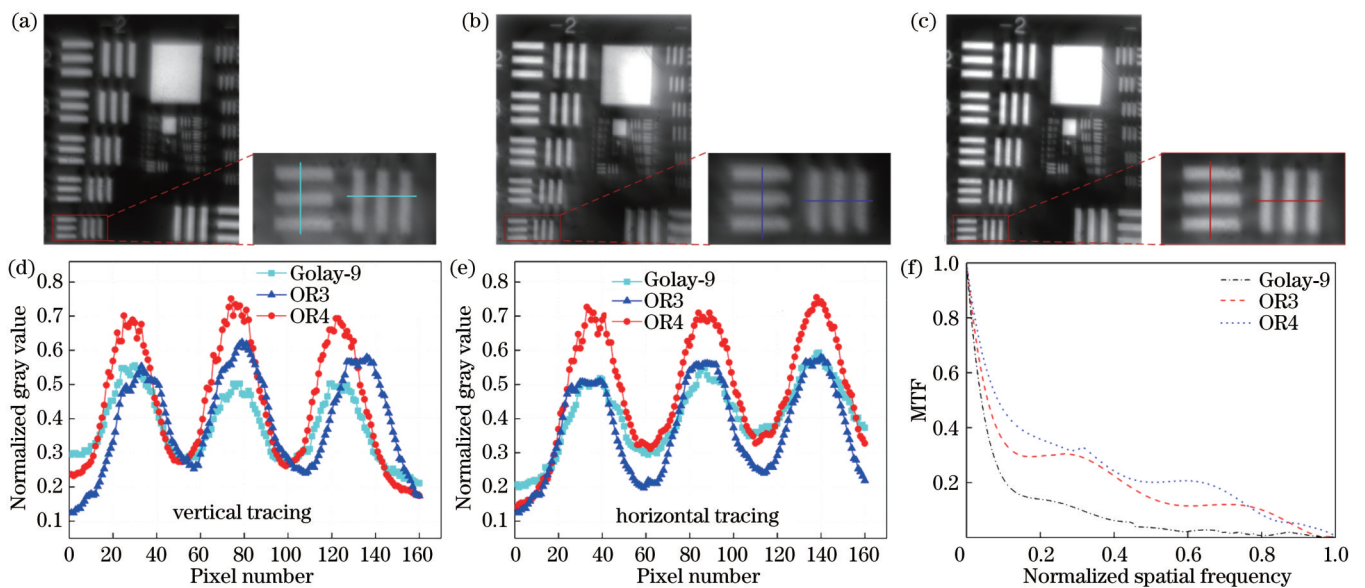


图 10 Golay-9、OR3 和 OR4 阵列结构的实验结果。(a)利用 Golay-9 结构得到的图像;(b)利用 OR3 结构得到的图像;(c)利用 OR4 结构得到的图像;(d)第 6 组横向线对的灰度追迹;(e)第 6 组纵向线对的灰度追迹;(f)MTF 估计

Fig. 10 Experimental results of Golay-9, OR3, and OR4 arrays. (a) Image obtained by Golay-9 array; (b) image obtained by OR3 array; (c) image obtained by OR4 array; (d) line traces of horizontal bars of group 6; (e) line traces of vertical bars of group 6; (f) MTF estimation

化,图 10(c)、(d)分别给出了第 6 组横杠和纵杠的线迹结果。横杠线对的归一化灰度差值(峰谷值之差)依次为:Golay-9 的差值是 0.2728、0.2309、0.2207,OR3 的差值是 0.2988、0.3548、0.3223,OR4 的差值是 0.5851、0.3693、0.4232。纵杠线对的归一化灰度差值依次为:Golay-9 的差值是 0.2291、0.2118、0.2223,OR3 的差值是 0.3172、0.3499、0.3387,OR4 的差值是 0.4522、0.4647、0.4270。差值越大,说明对比度越高,这些结果表明 OR4 和 OR3 阵列结构得到的图像质量高于 Golay-9 阵列的图像质量,证明了旋转合成孔径结构对稀疏孔径系统成像质量的改善是有效的。图 10(f)给出了经过 Golay-9、OR3 和 OR4 阵列所成图像的 MTF 估计曲线,可以看出,OR3 和 OR4 阵列的 MTF 均高于 Golay-9 阵列的,另外 OR3 和 OR4 阵列的 $M_{\text{mid-freq}}$ 分别为 0.1159 和 0.1501,均大于 Golay-9 阵列的 0.0699,这表明使用新的构型方法得到的旋转合成孔径阵列对提升中频 MTF 是有效的。

5 结 论

本文基于一维非冗余三孔径阵列设计了旋转合成孔径结构,在 360° 范围内以不同旋转角度进行多次旋转,使其能够覆盖更广的频域范围,并提高中频 MTF 和系统成像性能。与 Golay-9 阵列结构相比,OR3 阵列在 f_x 和 f_y 方向的整个频率范围内的 MTF 均高于 Golay-9 阵列的 MTF,而且 5 种旋转合成阵列除了实际截止频率小于 Golay-9 阵列的 0.8951,其余的三种评价指标均高于 Golay-9 阵列。根据实验结果,比较 Golay-9、OR4 和 OR3 阵列的 USAF1951 分辨率板图像的第 6 组横、纵杠线对的归一化灰度差值,Golay-9、OR3 和 OR4 阵列的最大差值分别为 0.2728、0.3548、0.5851 和 0.2291、0.3499、0.4647,差值越大则图像对比度越高,同时经过 OR3 和 OR4 阵列所成图像的 MTF 估计曲线均高于 Golay-9 阵列,且 OR3 和 OR4 阵列的 $M_{\text{mid-freq}}$ 值(0.1159 和 0.1501)均大于 Golay-9 阵列的 0.0699,这些结果证明了所提出的阵列结构设计方法的有效性。

参 考 文 献

- [1] Meinel A B. Cost-scaling laws applicable to very large optical telescopes[J]. *Optical Engineering*, 1979, 18(6): 645-647.
- [2] Redding D C, Basinger S A, Lowman A E, et al. Wavefront sensing and control for a Next-Generation Space Telescope[J]. *Proceedings of SPIE*, 1998, 3356: 758-772.
- [3] 周程灏,王治乐,张树青,等.大孔径衍射受限光学合成孔径系统 MTF 中频补偿[J]. *光学学报*, 2018, 38(4): 0411005. Zhou C H, Wang Z L, Zhang S Q, et al. Large aperture diffraction limited optical synthetic aperture system intermediate frequency MTF compensation[J]. *Acta Optica Sinica*, 2018, 38(4): 0411005.
- [4] Zhou C H, Wang Z L. Mid-frequency MTF compensation of optical sparse aperture system[J]. *Optics Express*, 2018, 26(6): 6973-6992.
- [5] 赵佳晨,张越,金科.振动对光学合成孔径的成像影响[J]. *光*

学学报, 2022, 42(22): 2211001.

- Zhao J C, Zhang Y, Jin K. Imaging effect of vibration on optical synthetic aperture[J]. *Acta Optica Sinica*, 2022, 42(22): 2211001.
- [6] 范君柳,吴泉英,陈宝华,等.基于双泽尼克多项式的多视场稀疏孔径成像[J]. *光学学报*, 2023, 43(10): 1011001. Fan J L, Wu Q Y, Chen B H, et al. Multi-field-of-view sparse aperture imaging based on double Zernike polynomials[J]. *Acta Optica Sinica*, 2023, 43(10): 1011001.
- [7] 徐焕宇,徐萌兮,余宇,等.自适应光学系统图像的梯度域点扩散函数估计与盲复原方法[J]. *激光与光电子学进展*, 2023, 60(4): 0401001. Xu H Y, Xu M X, She Y, et al. Gradient domain point spread function estimation and blind restoration of adaptive optical system images[J]. *Laser & Optoelectronics Progress*, 2023, 60(4): 0401001.
- [8] Flores J L, Paez G, Strojnik M. Design of a diluted aperture by use of the practical cutoff frequency[J]. *Applied Optics*, 1999, 38(28): 6010-6018.
- [9] Golay M J E. Point arrays having compact, nonredundant autocorrelations[J]. *Journal of the Optical Society of America*, 1971, 61(2): 272-273.
- [10] Fitch J P, Lawrence T W. Placement of multiple apertures for imaging telescopes[J]. *Proceedings of SPIE*, 1990, 1237: 61-69.
- [11] 钱霖,吴泉英,吴峰,等.复合三子镜的成像研究[J]. *光学学报*, 2005, 25(8): 1030-1035. Qian L, Wu Q Y, Wu F, et al. Study on imaging of dual three sub-apertures design[J]. *Acta Optica Sinica*, 2005, 25(8): 1030-1035.
- [12] 郝未倩,梁忠诚,刘肖尧,等.分形结构稀疏孔径阵列的成像性能[J]. *物理学报*, 2019, 68(19): 199501. Hao W Q, Liang Z C, Liu X Y, et al. Imaging performance of fractal structure sparse aperture arrays[J]. *Acta Physica Sinica*, 2019, 68(19): 199501.
- [13] 赵娟,王大勇,张亚新,等.光学稀疏孔径系统复合阵列构造对系统成像的影响[J]. *中国激光*, 2009, 36(4): 934-939. Zhao J, Wang D Y, Zhang Y X, et al. Effect of different designs of the multiple-array configuration on imaging of optical sparse aperture systems[J]. *Chinese Journal of Lasers*, 2009, 36(4): 934-939.
- [14] 刘肖尧,梁忠诚,郝未倩,等.辐射状多子镜阵列结构的成像特性[J]. *光学学报*, 2019, 39(8): 0811003. Liu X Y, Liang Z C, Hao W Q, et al. Imaging characteristics of radial multi-sub-mirror array[J]. *Acta Optica Sinica*, 2019, 39(8): 0811003.
- [15] 易红伟,李英才,樊超.稀疏孔径等边六孔径结构研究[J]. *光子学报*, 2007, 36(11): 2062-2065. Yi H W, Li Y C, Fan C. Research on pupil configuration of equilateral six sub-apertures sparse-aperture system[J]. *Acta Photonica Sinica*, 2007, 36(11): 2062-2065.
- [16] 魏小峰,耿则勋,曹力,等.一种新的光学合成孔径系统成像性能指标与光瞳优化方法[J]. *光学学报*, 2014, 34(11): 1111001. Wei X F, Geng Z X, Cao L, et al. A novel imaging performance index and pupil optimization method for optical synthetic aperture system[J]. *Acta Optica Sinica*, 2014, 34(11): 1111001.
- [17] 梁士通,杨建峰,李湘沅,等.一种新型稀疏孔径结构的研究[J]. *光子学报*, 2010, 39(1): 148-152. Liang S T, Yang J F, Li X J, et al. Study of a new sparse-aperture system[J]. *Acta Photonica Sinica*, 2010, 39(1): 148-152.
- [18] Guyon O, Roddier F. Aperture rotation synthesis: optimization of the (u, v) -plane coverage for a rotating phased array of telescopes[J]. *Publications of the Astronomical Society of the Pacific*, 2001, 113(779): 98-104.
- [19] Liu L, Jiang Y S, Wang H Y, et al. Novel array configuration

- and its optimization for sparse aperture imaging systems[J]. *Optical Engineering*, 2011, 50(5): 053202.
- [20] 李莉文, 梁忠诚, 赵瑞, 等. 光学合成孔径的多目标模拟退火阵列优化[J]. *激光与光电子学进展*, 2021, 58(16): 1611001.
Li L W, Liang Z C, Zhao R, et al. Optimization of multiobjective simulated annealing array for optical synthetic aperture[J]. *Laser & Optoelectronics Progress*, 2021, 58(16): 1611001.
- [21] Chen K S, He Z S, Han C L. Design of 2-dimension sparse arrays using an improved genetic algorithm[C]//Fourth IEEE Workshop on Sensor Array and Multichannel Processing, July 12-14, 2006, Waltham, MA, USA. New York: IEEE Press, 2008: 209-213.
- [22] Chen K S, Yun X H, He Z S, et al. Synthesis of sparse planar arrays using modified real genetic algorithm[J]. *IEEE Transactions on Antennas and Propagation*, 2007, 55(4): 1067-1073.
- [23] Salvaggio P S, Schott J R, McKeown D M. Genetic apertures: an improved sparse aperture design framework[J]. *Applied Optics*, 2016, 55(12): 3182-3191.
- [24] Liu A M, Gao L M, Xiao M S. Improved multiple circular array configuration for sparse aperture optical imaging systems[J]. *Optical Engineering*, 2017, 56(7): 073109.
- [25] Cassaing F, Mugnier L M. Optimal sparse apertures for phased-array imaging[J]. *Optics Letters*, 2018, 43(19): 4655-4658.
- [26] 蔡宏, 耿安兵. 基于混合算法的光学合成孔径成像系统孔径优化[J]. *光学与光电技术*, 2012, 10(2): 65-68.
Cai H, Geng A B. Aperture optimization of optical synthetic aperture imaging system based on hybrid algorithm[J]. *Optics & Optoelectronic Technology*, 2012, 10(2): 65-68.
- [27] Zhao W X, Zhang X F. End-to-end aperture layout optimization and image restoration for optical sparse aperture systems[J]. *Optics Letters*, 2023, 48(10): 2504-2507.

Imaging Characteristics of One-Dimensional Rotating Synthetic Array for Sparse Aperture

Zhang Huiyan^{1,2}, Liu Ming^{1,2*}, Ning Bu^{1,2,3}, Hui Mei^{1,2}, Dong Liquan^{1,2,3}, Kong Lingqin^{1,2},
Zhao Yuejin^{1,2}

¹*School of Optics and Photonics, Beijing Institute of Technology, Beijing 100081, China;*

²*Beijing Key Laboratory for Precision Optoelectronic Measurement Instrument and Technology, Beijing 100081, China;*

³*Yangtze Delta Region Academy of Beijing Institute of Technology, Jiaxing 314019, Zhejiang, China*

Abstract

Objective Optical sparse aperture (OSA) imaging system is composed of multiple discrete circular sub-apertures, which attempts to obtain a resolution approximately equivalent to a single filled large aperture system with reduced size, cost, and weight. However, compared with a single aperture system, the performance of these sparse arrays strongly relies on various design parameters, such as the number of sub-apertures, their relative positions, and diameters. Due to the discreteness and sparsity of the sparse aperture array, the pupil function is no longer a connected domain, which further reduces the intermediate frequency modulation transfer function (MTF), thus degrading images. To address this issue and enhance the intermediate frequency MTF while improving the imaging quality, a one-dimensional non-redundant three-aperture structure with a sub-aperture spacing ratio of 1:2 is selected as a foundational array, and the position of the middle sub-aperture is fixed. Then a novel rotating synthetic aperture structure is designed by rotating the base array several times along the baseline direction at different angles within 360°. Both quantitative and qualitative evaluations of simulation and experimental results demonstrate the effectiveness of the proposed method.

Methods The pupil autocorrelation distribution of one-dimensional multi-aperture arrays is first analyzed. Since the three-aperture structure with a center distance ratio of 1:2 of two sub-apertures can obtain greater frequency domain coverage with fewer rotation times and a smaller filling factor, this structure is selected as the fundamental array. To create a new synthetic aperture structure, this three-aperture array is rotated by an angle α along the baseline direction around the intermediate sub-aperture. To ensure adherence to the design requirements of the sparse aperture array and prevent overlap between any two sub-apertures in space, various constraint conditions for structural parameters are computed. These constraints encompass parameters such as the center spacings (s_1 and s_2) of the two sub-apertures, the rotation angle α , and the center position coordinates of the rotated sub-apertures. In addition, the pupil function, point spread function (PSF), and MTF of the rotated arrays are derived. The imaging characteristics of the array structure synthesized by a single rotation are simulated. Notably, the MTF frequency domain coverage of the rotating synthetic aperture is not a simple sum of two directions but rather an expansion, and PSF changes from fringe distribution in one direction to speckle and linear distribution in different directions. In order to increase the coverage of the rotating synthetic aperture in the whole

frequency domain, rotation is repeated multiple times to synthesize new apertures. Specifically, the rotation within 360° is performed six times per $2\pi/7$, five times per $\pi/3$, four times per $2\pi/5$, three times per $\pi/2$, and two times per $2\pi/3$, respectively. The obtained arrays are denoted as OR6, OR5, OR4, OR3, and OR2, respectively.

Results and Discussions According to the theoretical model, with the increase in the single rotation angle in Fig. 4, the energy of MTF and PSF is mainly concentrated in the central region. The sidelobe energy of MTF is continuous along two directions of the pupil structure and gradually presents a point-like discrete distribution in other directions, covering a wider range of frequency domains. Figure 6 shows the pupil structure, as well as the PSF and MTF distributions of Golay-9 and five rotating synthetic arrays. As the number of rotations decreases, the MTF frequency domain coverage of the rotating synthetic aperture becomes smaller and presents a discrete distribution. The PSF energy of the OR6 array is almost all concentrated in the center, which is close to the PSF distribution of the single aperture. The PSF sidelobe of the OR5 and OR4 arrays is converged toward the center. However, the PSF energy distribution of OR3 and OR2 arrays is more discrete, and the sidelobe energy is continuously enhanced. At the same equivalent diameter, the MTF distribution in the Golay-9 array is relatively uniform, but its intensity is low in the middle and high frequency bands, and the PSF presents a discrete circular spot distribution, which degrades the image. In the f_x direction in Fig. 7, the MTFs of OR5 and OR3 arrays in the frequency range of 0.4–1.0 are close to that of equivalent single aperture and is higher than that of Golay-9 arrays in the whole spatial frequency range. Moreover, the MTF of OR6, OR4, and OR2 arrays in the frequency range of 0.18–0.6 is higher than that of Golay-9. In the f_y direction, the MTFs of four rotating synthetic arrays are greater than that of the Golay-9 array in the frequency range of 0.2–0.6, and the MTF of the OR3 array in the frequency range of 0.15–1.0 is greater than that of the Golay-9 array. At the same equivalent diameter, $M_{\text{mid-freq}}$, peak signal-to-noise ratio, and structural similarity of rotating synthetic aperture arrays are higher than that of the Golay-9 array.

Conclusions In this study, the rotating synthetic aperture arrays for improving intermediate frequency MTF and image performance are proposed, which are obtained by rotating a one-dimensional non-redundant three-aperture array several times at different rotation angles within 360° . The MTF of the OR3 array surpasses that of the Golay-9 array across the entire frequency range in both the f_x and f_y directions. However, three evaluation indexes of the five rotating synthetic arrays are higher than those of the Golay-9 array. According to the experimental results, the normalized gray difference values of the sixth group of horizontal and vertical bar pairs of USAF1951 resolution board images of Golay-9, OR4, and OR3 arrays are compared. The maximum difference values of Golay-9, OR3, and OR4 arrays are 0.2728, 0.3548, 0.5851 for horizontal lines, as well as 0.2291, 0.3499, and 0.4647 for vertical lines, respectively. A higher difference implies greater image contrast. Moreover, the MTF estimation of OR3 and OR4 arrays is higher than that of the Golay-9 array, which proves the validity of the proposed array structure design method.

Key words imaging systems; optical sparse aperture; one-dimensional multi-aperture array; rotating synthesis; intermediate frequency modulation transfer function; frequency domain coverage